# Electronic Supplementary Information

## Bimetallic sulfide NiCo₂S₄ yolk-shell nanospheres as

## high-performance cathode materials for rechargeable magnesium

## batteries

Yiming Ma[a,1,*], Yujie Zhang[b,1], Fan Wang[c], Haijiao Xie[d] and Jin Wang[a]

[a] *State Key Laboratory of Advanced Electromagnetic Engineering and Technology, School of Electrical and Electronic Engineering, Huazhong University of Science and Technology, Wuhan 430074, P. R. China*

[b] *State Key Laboratory of Materials Processing and Die & Mould Technology, School of Materials Science and Engineering, Huazhong University of Science and Technology, Wuhan 430074, P. R. China*

[c] *School of Resource and Environmental Sciences, Hubei International Scientific and Technological Cooperation Base of Sustainable Resource and Energy, Wuhan University, Wuhan, 430072, P. R. China*

[d] *Hangzhou Yanqu Information Technology Co., Ltd., Hangzhou 310003, P.R. China*

\* Corresponding author.
*E-mail addresses:* mayiming@hust.edu.cn

Y. Ma and Y. Zhang contributed equally to this work.

## Materials and methods

**Syntheses of NiCo-glycerol and Co-glycerol solid spheres:** The synthesis of NiCo-glycerol was according to previous reports.[1] In a typical synthesis, 1 mmol $Co(NO_3)_2 \cdot 6H_2O$, 0.5 mmol $Ni(NO_3)_2 \cdot 6H_2O$, and 32 mL of glycerol were dispersed in 160 mL isopropanol. After stirring for over 120 min, the mixture was transferred to a 200 mL Teflon-lined stainless-steel autoclave and maintained at 180 °C for 6 h. Then the solid product was washed with ethanol and dried under vacuum at 60 °C for over 24 h. The synthesis of Co-glycerol solid spheres was the same as the synthesis procedure of NiCo-glycerol solid spheres only substituting $Ni(NO_3)_2 \cdot 6H_2O$ for 0.5 mmol $Co(NO_3)_2 \cdot 6H_2O$.

**Syntheses of yolk-shell $NiCo_2S_4$ (NCS) and yolk-shell $Co_3S_4$ (CS):** 240 mg of the as-prepared NiCo-glycerol/Co-glycerol and 400 mg thioacetamide (TAA) were were dispersed in 160 mL ethanol via sonication for 120 min. The mixture was transferred to a 200 mL Teflon-lined stainless-steel autoclave and maintained at 180 °C for 6 h.

**Preparation of NCS and CS electrodes:** The as-prepared NCS/CS powder was mixed with Super P and polyterafluoroethylene binder (PTFE) with a weight ratio of 8:1:1 in isopropanol solvent. Then the slurry was spread onto carbon cloth l with the areal mass loading ~1.2 mg cm$^{-2}$. The electrodes were dried out at 70 °C under vacuum for overnight.

**Preparation of 0.5 M Mg-HMDS/G4 electrolyte:** The synthesis of 0.5 M Mg-HMDS/G4 electrolyte was according to previous reports.[2,3] Typically, 0.5 mmol $Mg(HMDS)_2$ (Sigma-Aldrich) and 1 mmol $AlCl_3$ (Alfa asear) were dissolved in 1 mL

tetraglyme (G4) with stirring for 24 h. Then, 0.5 mmol $MgCl_2$ was added into the electrolyte with stirring for over 7 days.

**Structural characterization**

The morphology and structure were characterized via the scanning electron microscopy (Zeiss Sigma 300), transmission electron microscope (JEOL JEM 2100F), X-ray diffraction (X'Pert PRO MPD), Raman (LabRam HR Evolution), Brunauer-Emmett-Teller (BET) adsorption-desorption analysis (Micromeritics ASAP 2460) and X-ray Photoelectron Spectroscopy (XPS, Thermo Kalpha). For the Mg-storage mechanism investigation, cycled cells were opened in the glovebox (O2 and H2O < 0.1 ppm), and the cycled electrodes were washed with Tetrahydrofuran (THF, anhydrous) before the measurements.

**Electrochemical characterization**

All the electrochemistry analyses were carried out based on 2032 coin-type cells assembled in the glove box filled with Ar. For electrolyte characterization, different collectors (Al, Mo, Cu, and Carbon paper), Mg foil after polished and glass fiber were used as working electrode, counter electrode, and separator respectively. For half-cell characterization, NCS/CS electrode, Mg foil after polished, and glass fiber were used as cathode, anode/counter electrode, and separator respectively. An 18mm diameter molybdenum foil current collector separates the corrosive electrolyte from the stainless steel can, ensuring the coin cell electrochemical stability. Galvanostatic charge/discharge tests were carried out using a NEWARE battery testing system. Cyclic voltammetry (CV) was analyzed with CHI 660e electrochemical workstation.

**Computational section**

The DFT calculations were performed in the Vienna ab initio simulation package (VASP).[4] A spin-polarized GGA PBE functional, all-electron plane-wave basis sets with an energy cut-off of 520 eV, and a projector augmented wave (PAW) method were adopted.[5] A (3 × 3 × 1) Monkhorst-Pack mesh was used for the Brillouin-zone integrations to be sampled. The conjugate gradient algorithm was used in the optimization. The convergence threshold was set 1*10-4 eV in total energy and 0.05 eV/ Å in force on each atom. The crystal information file (CIF) and the initial cell parameters for the $NiCo_2S_4$ and $Co_3S_4$ are available from the Cambridge crystallographic data centre (CCDC) software.[6]

**Kinetics investigation**

The Mg-ion diffusion coefficient was calculated using the Randles-Sevcik equation:

$$I\text{p} \ = \ 2.69 \times 10^5 n^{\frac{3}{2}} A D^{\frac{1}{2}} v^{\frac{1}{2}} C_{Mg^{2+}} \tag{1}$$

Where $I_p$ is the peak current, $n$ is the transferring electron numbers, $A$ is the connecting area of electrolyte, $D$ is the $Mg^{2+}$ diffusion coefficient, $v$ is the scan rate and $C$ is the concentration of $Mg^{2+}$ ions.

**Pseudocapacitance contribution calculation**

The surface-controlled pseudocapacitive behaviors could be evaluated according to the equation:

$$i(\text{V}) = k_1 v + k_2 v^{1/2} \tag{2}$$

Where $i(\text{V})$ is the total current at the corresponding fixed potential V, $k_1 v$ is

capacitive contribution and $k_2v^{1/2}$ is diffusion contribution.
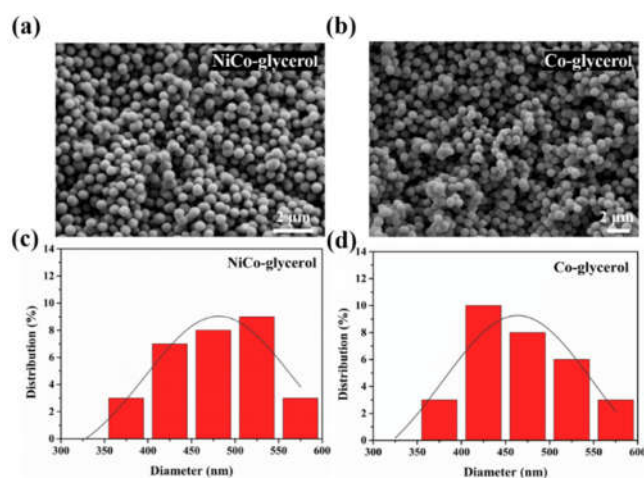
# Figures and Tables



**Fig. S1.** SEM images of the (a) NiCo-glycerol and (b) Co-glycerol precursors.

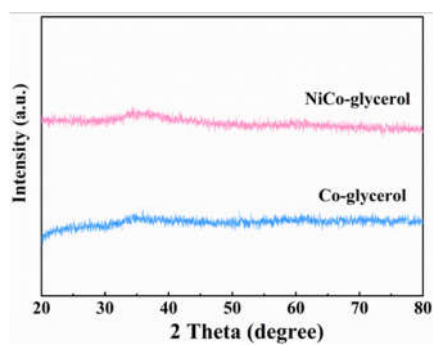Particle size distribution of the (c) NiCo-glycerol and (d) Co-glycerol precursors.



**Fig. S2.** XRD patterns of the NiCo-glycerol and Co-glycerol precursors.
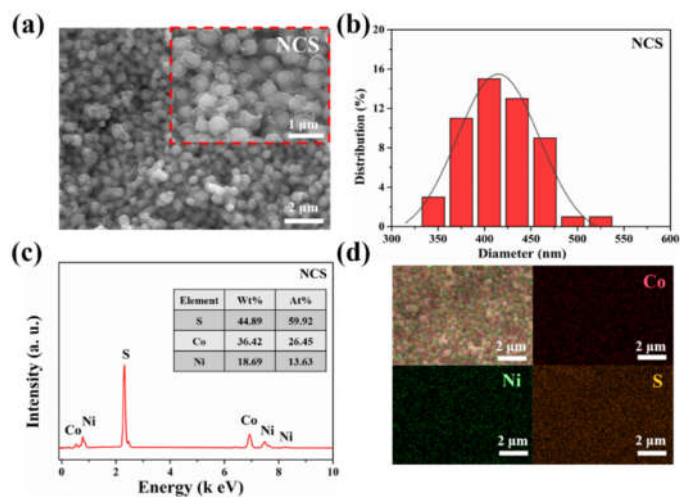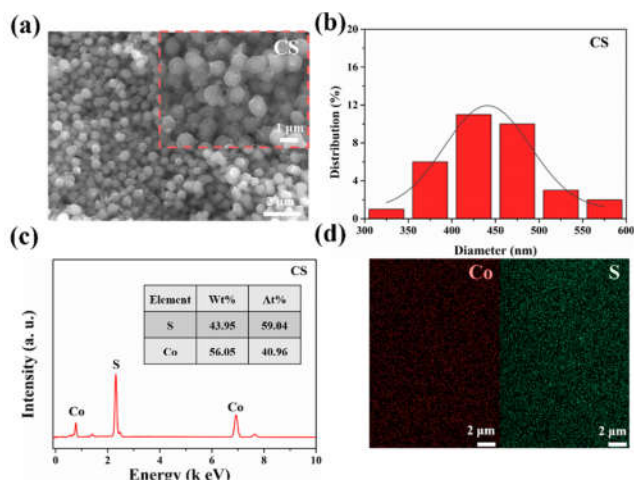
**Fig. S3.** (a) SEM images of the yolk-shell $NiCo_2S_4$ (NCS) nanospheres and (b) corresponding particle size distribution. (c) EDS spectra and (d) corresponding elemental mapping of the NCS.



**Fig. S4.** (a) SEM images of the yolk-shell $Co_3S_4$ (CS) nanospheres and (b) corresponding particle size distribution. (c) EDS spectra and (d) corresponding elemental mapping of the CS.
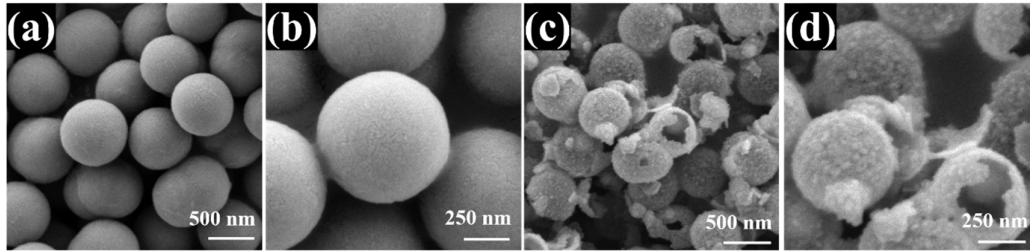
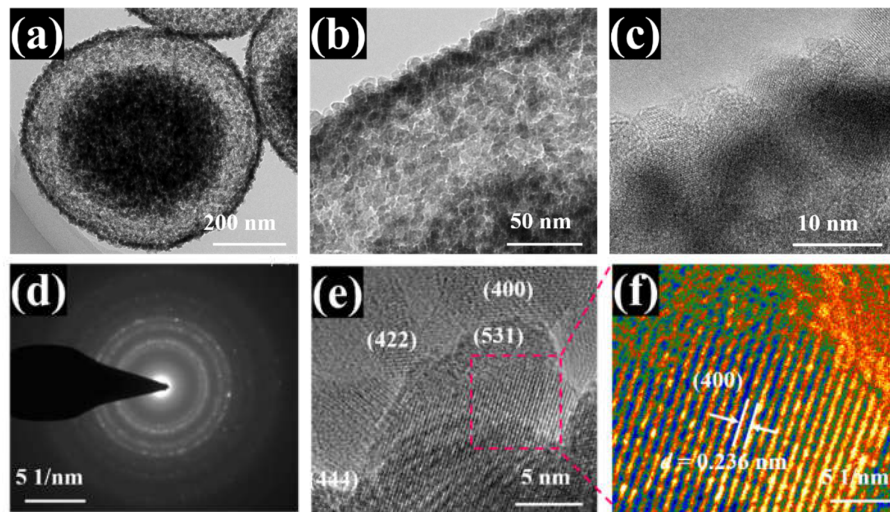**Fig. S5.** SEM images of the yolk-shell $Co_3S_4$ (CS) nanospheres.



**Fig. S6.** (a-c) TEM, (d) SAED and (e, f) HRTEM images of the CS.
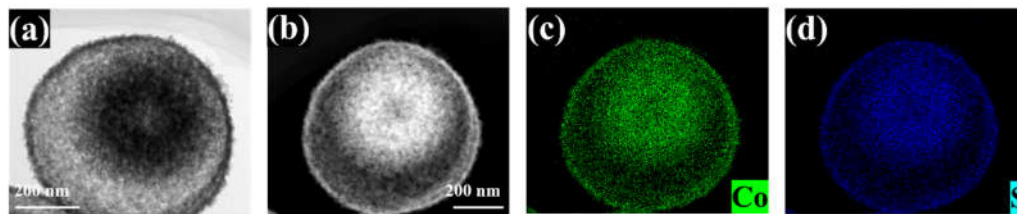
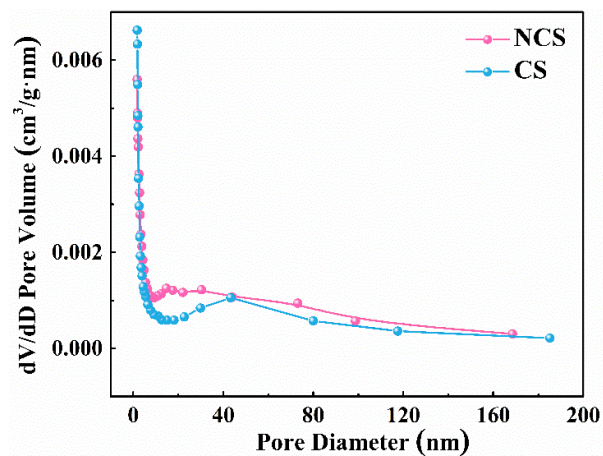**Fig. S7.** . (a) TEM, (b) STEM, and (c, d) elements mapping of the CS.



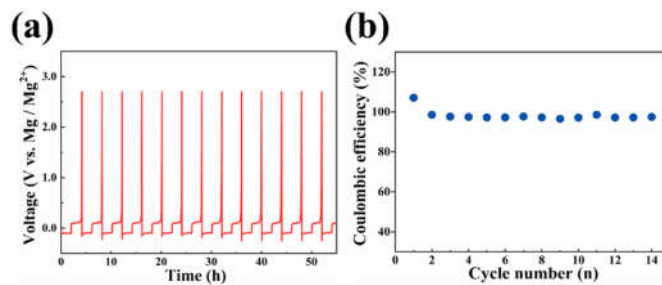**Fig. S8.** The distribution of pore size for NCS and CS samples.

**Fig. S9.** (a) Mg deposition−stripping curves of the 0.5 M Mg-HMDS/G4 electrolyte in the two-electrode coin cell with molybdenum collector, the upper limit of charge voltage being 2.7 V. (b) Corresponding deposition−stripping cycling coulombic efficiency.
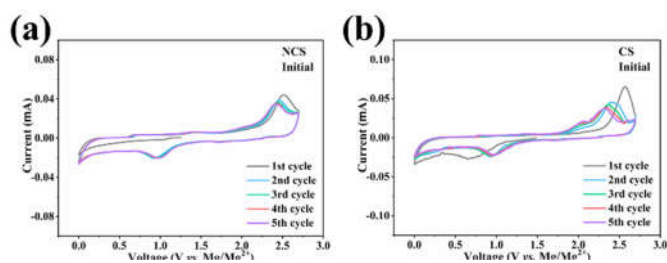


**Fig. S10.** CV curves of (a) yolk-shell NiCo$_2$S$_4$ (NCS) and (d) Co$_3$S$_4$ (CS) for the initial five cycles.
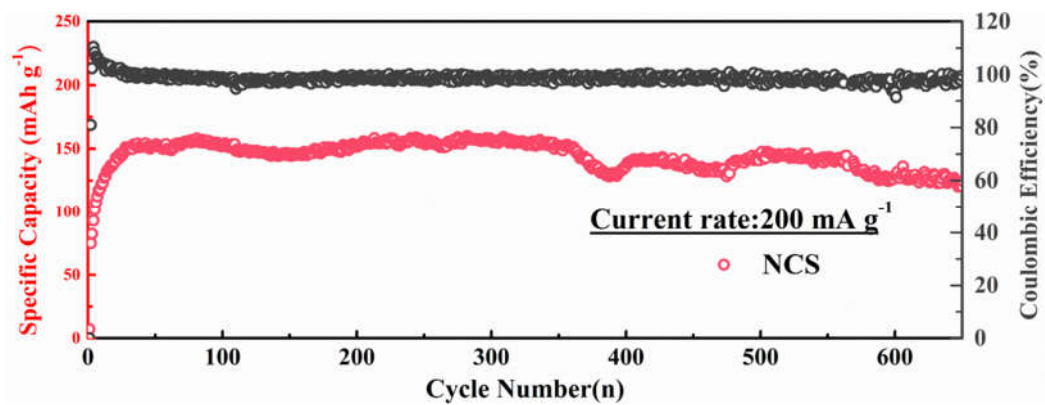
**Fig. S11.** Cycling performance of the NCS and CS cathdoes at current densitiy at 200 mA g$^{-1}$ for initial 650 cycles.
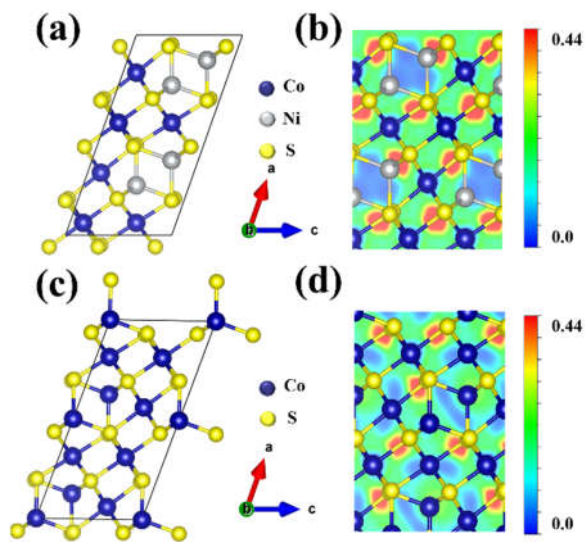


**Fig. S12.** Crystal structure of (a) NiCo$_2$S$_4$ and (c) Co$_3$S$_4$. Corresponding electron density difference map for (b) NiCo$_2$S$_4$ and (d) Co$_3$S$_4$.
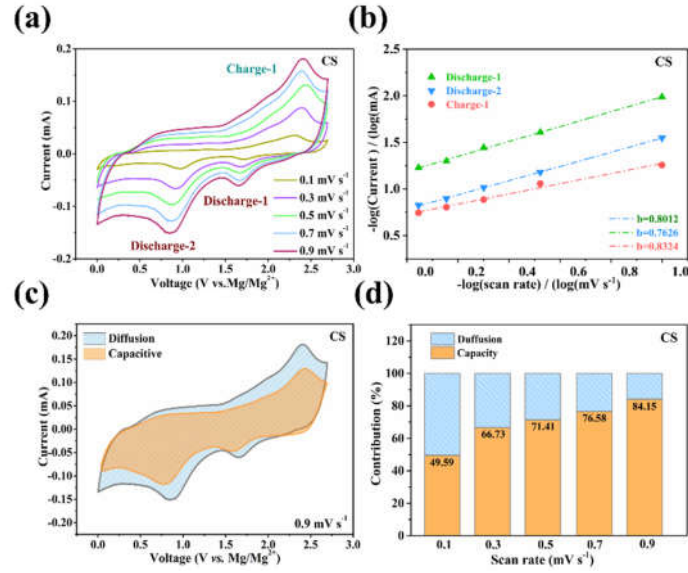
**Fig. S13.** (a) CV curves of the CS electrodes at various scan rates from 0.1 to 0.9 mV s$^{-1}$ and (b) corresponding plots of –log $i$ versus –log $v$ at specific peak rates. (c) CV curves with capacitive contribution of CS at 0.9 mV s$^{-1}$ and (d) corresponding capacitive-controlled capacity contributions at various scan rates from 0.1 to 0.9 mV s$^{-1}$.

**Table S1.** Summary of the representative cathode materials electrochemical performance for Mg batteries reported in recent literature.

| Materials | Voltage (V) | Capacity (mAh g⁻¹) | Cycling stability | Ref. |
|---|---|---|---|---|
| $\zeta$-$V_2O_5$ | 2 | 130 | 15 | 7 |
| $Na_2V_6O_{16}\cdot1.63H_2O$ | 2.4 | 250 | 450 | 8 |
| $Ag_2S$ | 2, 1.3 | 100 | 400 | 9 |
| $NiCo_2Se_4$ | 1.0 | 145 | 1000 | 10 |
| CuS | 1.1 | 200 | 350 | 11 |
| $Mo_6S_8$ | ~1.1 | 82 | 20 | 12 |
| $Mo_6S_8$ | 1.2, 0.8 | 120 | 50 | 13 |
| **$NiCo_2S_4$** | **1.5, 0.9** | **275** | **400** | **This work** |

# Notes and references

1   L. Shen, L. Yu, H. B. Wu, X. Yu, X. Zhang and X. Lou, *Nat. Commun.*, 2015, **6**, 6694.

2   Z. Zhao-karger, X. Zhao, D. Wang, T. Diemant, R. J. Behm and M. Fichtner, *Adv. Energy Mater.*, 2015, **5**, 1401155.

3   H. Tian, T. Gao, X. Li, X. Wang, C. Luo, X. Fan, C. Yang, L. Suo, Z. Ma, W. Han and C. Wang, *Nat. Commun.*, 2017, **8**, 14083.

4   G. Kresse and J. Furthmuller, *Phys. Rev. B*, 1996, **54**, 11169-11171.

5   J. P. Perdew, K. Burke and M. Ernzerhof, *Phys. Rev. Lett.*, 1996, **77**, 3865-3866.

6   C. R. Groom and F. H. Allen, *Angew. Chem. In. Ed.*, 2014, **53**, 1306438.

7   I. D. Johnson, G. Nolis, L. Yin, H. D. Yoo, P. Parajuli, A. Mukherjee, J. L. Andrews, M. Lopez, R. F. Klie, S. Banerjee, B. J. Ingram, S. Lapidus, J. Cabana and J. A. Darr, *Nanoscale*, 2020, **12**, 22150–22160.

8   R. Sun, X. Ji, C. Luo, S. Hou, P. Hu, X. Pu, L. Cao, L. Mai and C. Wang, *Small*, 2020, **16**, 2000741.

9   Y. Zhang, X. Li, J. Shen, Z. Chen, S. Cao, T. Li and F. Xu, *Dalton Trans.*, 2019, **48**, 14390–14397.

10  Y. Zhang, T. Li, S. Cao, W. Luo and F.Xu, *ACS Sustainable Chem. Eng.*, 2020, **8**, 2964−2972.

11  M. Wu, Y. Zhang, T. Li, Z. Chen, S. Cao and F. Xu, *Nanoscale*, 2018, **10**, 12526–12534.

12  F. Murgia, P. Antitomaso, L. Stievano, L. Monconduit and R. Berthelot, *J. Solid State Chem.*, 2016, **242**, 151–154.

13  S. Woo, J. Yoo, W. Cho, M. Park. K. J. Kim, J. Kim, J. Kim and Y. Kim, *RSC Adv.*, 2014, **4**, 59048–59055.